J Appl Electrochem (2007) 37:843–852
DOI 10.1007/s10800-007-9320-6

ORIGINAL PAPER

Multicriteria optimization of mechanical and morphological properties of chromium electrodeposits under reverse pulse plating

L. Hallez · M. De Petris-Wery · M. Assoul · M. Feki · H. F. Ayedi

Received: 23 November 2006 / Accepted: 27 February 2007 / Published online: 27 March 2007

Abstract In this work, a central composite design experiment was performed to estimate the effect of the electroplating parameters (temperature of electrolyte, cathodic and anodic pulse current densities, and cathodic and anodic pulse lengths,) on four properties of hard chromium electrodeposits. The studied responses were the hardness (Hv), the roughness quantified by the two criteria R_a (nm) and R (μm)), and the specific abrasive energy, E_s (μJ μm^{-3}). Analysis of the responses using optimal path technique did not lead to a common set of experimental conditions which fulfilled the required properties. Thus, the desirability function approach has been employed in order to find the best compromise between the different experimental responses. The optimal conditions are: electrolyte temperature: 49.9 °C; cathodic pulse current density: 42.0 A dm^{-2}; anodic pulse current density: 51.5 A dm^{-2}, cathodic pulse length: 6.23 s and anodic pulse length: 28.5 ms. Under these conditions, the estimated response values are 738 Hv, 262 nm, 2.61 μm and 0.027 μJ μm^{-3} for hardness, R_a, R and specific abrasive energy respectively, validated experimentally. The resultant coating, examined by AFM, exhibits a nodular fine-grained morphology.

Keywords Hard chromium · Pulse reverse plating · Roughness · Specific abrasive energy · Central composite design · Desirability

L. Hallez · M. De Petris-Wery (✉)
Laboratoire de Chimie des Matériaux et des Interfaces, Université de Franche-Comté, Route de Gray, 25030 Besancon, France
e-mail: martine.wery@iut-orsay.fr

M. De Petris-Wery
IUT d'Orsay, Université de Paris XI, Plateau du Moulon, 91400 Orsay, France

L. Hallez · M. Assoul
Laboratoire de Microanalyses des Surfaces, Ecole Nationale Supérieure de Micromécanique et de Microtechniques, Rue de l'Epitaphe, 25030 Besancon, France

M. Feki · H. F. Ayedi
URCIM – Ecole Nationale d'Ingénieurs de Sfax, BP W, 3038 Sfax, Tunisie

1 Introduction

Electrodeposited hard chromium has gained an outstanding position in industry for its unique combination of wear characteristics and/or corrosion resistance at low cost. Currently many industrial fields, such as the automotive, aerospace, mining, and general engineering, industries have adopted electrodeposited hard chromium parts [1–4]. The thickness of the hard deposit varies markedly with the application but is usually in the range 20–500 μm which is appreciably thicker than that used for decorative chromium (1 μm). Hard chromium is commonly produced from chromic acid solutions, being fluoride free and containing catalytic anions such as sulphates, at high current density (20–50 A dm^{-2}). In these operating conditions, the current efficiency is low (10–20%) because of hydrogen evolution and reduction of chromium (VI) to chromium (III) species [5–7]. More than 50% of the electric charge is consumed by the unwanted hydrogen and oxygen evolved on the cathode and anode respectively.

Several investigations have been carried out to determine the effects of experimental factors such as plating temperature and current density, on current efficiency and coating properties such as microstructure, abrasion and corrosion resistance [8–18]. Furthermore, a modification of

the polarisation form (i.e. discontinuous with or without inversion of current) presents several advantages. Compared to direct current (DC) plating, pulse current (PC) techniques offer the availability of additional process factors, which can be varied independently, and the possibility of achieving higher instantaneous current densities [15–18]. Leisner et al. have demonstrated that the use of low frequency periodic current reversal of short duration during the deposition process can increase the current efficiency in the sulphate catalysed chromium bath and strongly influences the deposit structure [19–21]. Pulsed plated chromium is often observed to have a crack-free structure and lower hardness than chromium conventionally produced by DC because of the low residual stress in the deposit.

Although a considerable literature exists concerning pulse plating technology [22–27], there is relatively limited research dealing with the tribological and surface properties of chromium layers deposited with this technique [28, 29]. The evaluation of the factor range for reversal pulse plating (RPP) is difficult due to the numerous factors involved (Fig. 1). When RPP is used, cathodic and anodic current densities, cathodic (on time) and anodic (reverse on) times as well as temperature can be varied independently, forming a five-fold parameter space. Even though some investigations have employed statistical methods to optimise pulse-factors, these have been limited to optimisation of the current efficiency during hard chromium electrodeposition [19, 20].

The aim of the present work is to study the wear resistance and surface microgeometric properties of hard chromium electrodeposit under RPP using a chemiometrics approach [30–35]. It is based on the use of experimental design, which allows the simultaneous variation of all experimental studied factors. To this end, a second order design at five levels, based on fractional factorial design 2^{5-1}, was conducted to check the effects of the plating bath temperature and four factors characterising the reversal pulsing wave on the properties of the chromium coating: hardness, roughness and specific abrasive energy.

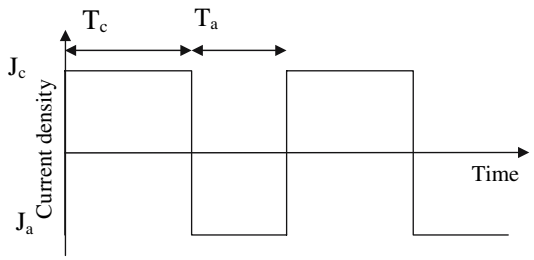

Fig. 1 Reversal pulse plating wave defined by J_c (A dm^{-2}): cathodic pulse current density, T_c (s): on time or cathodic pulse length, J_a (A dm^{-2}): anodic pulse current density and T_a (ms): reverse on time or anodic pulse length

Furthermore, the desirability function approach was applied to optimize the process under study in terms of maximisation of the hardness and the specific abrasive energy and minimization of the roughness [33–36].

2 Methodology and design of experiments

Experimental designs reduce the number of experiments in comparison with the traditional methodology, and provide information about how factors interact in a way that the method of one factor at a time cannot determine.

A factorial portion of a central composite design was set up to check the effects of the input variables and their interactions on the properties of the chromium coating. The variables U_j selected were:

- U_1: Temperature of the plating bath (°C)
- U_2: Cathodic pulse current density J_c (A dm^{-2})
- U_3: On time or cathodic pulse length T_c (s)
- U_4: Anodic pulse current density J_a (A dm^{-2})
- U_5: Reverse on time or anodic pulse length T_a (ms),

As currently used in experimental design, natural variables U_j were transformed into coded variables X_j [30–35]. For this design, each factor, X_j, is encountered at five levels ($-\alpha$, –1, 0, +1, + α). To achieve a rotatable design, α has to be set to 2 [33–35]. In addition, five replicates are needed at the centre point to look for the uniform precision property [33–35]. These replicates also permit calculation of an independent estimation of the pure experimental error variance. It should be noted that the principles governing the construction of this experimental design can be found in the specialised literature [33–35]. In order to define the experimental domain explored, the level values of variables were selected based on realistic limits for common pulse plating (Table 1). The output studied responses, noted Y_1, Y_2, Y_3 and Y_4, were respectively: the hardness (Hv), the roughness quantified by the two criteria (R_a (nm) and R (μm)), and the specific abrasive energy, E_s(μJ μm^{-3}).

A second-order model with 21 coefficients, including interaction terms, was assumed to describe the relationship between each response Y_i and experimental factors X_j:

Table 1 Study domain for the studied factors

Variables	Number of levels	Center $U_j(0)$	Step ΔU_j
U_1/°C	5	50	7.5
U_2/A dm^{-2}	5	42	6
U_3/s	5	9	4
U_4/A dm^{-2}	5	42	6
U_5/ms	5	30	10

$$Y_i = b_0 + b_1X_1 + b_2X_2 + b_3X_3 + b_4X_4 + b_5X_5 + b_{11}X_1^2 + b_{22}X_2^2 + b_{33}X_3^2 + b_{44}X_4^2 + b_{55}X_5^2 + b_{12}X_1X_2 + b_{13}X_1X_3 + b_{14}X_1X_4 + b_{15}X_1X_5 + b_{23}X_2X_3 + b_{24}X_2X_4 + b_{25}X_2X_5 + b_{34}X_3X_4 + b_{35}X_3X_5 + b_{45}X_4X_5 + e_i$$

where b_0 is the constant of the model, b_j the first degree coefficients, b_{jk} the cross-products coefficients, b_{jj} the quadratic coefficients and e_i the random .

The estimation of the model coefficients required 21 trials. However 31 trials have been carried out in order to estimate the factor effect, the pure error and the lack of fit, and then to be able to apply statistical tests to validate the models.

In this study, we were faced with five design variables. Rather than using a classical representation commonly employed in the Response Surface Methodology (RSM) as a contour plot (or three-dimensional plot), we chose to rely on the methodology of ridge analysis. The principle of this method is to determine the optimum path of the response surface by tracing spherical surfaces, centred on the central point of the experimental domain and with growing radius, and calculating for each of these the maximum and the minimum of the response surface. The output of the analysis is a set of coordinates of maxima or minima along with the predicted response, Y, at each computed point of the path [31, 33–35].

As one might expect, the optimum values (maxima or minima) for the responses do not occur at the same operating conditions but rather at widely separated points in the studied domain. This means that one must look for a compromise between conflicting criteria. Therefore, the optimization of the chromium coating properties requires a multicriteria decision making approach. This has been accomplished using Derringer's desirability function [36]. In short, the i estimated responses, i = 1–4, are transformed to a dimensionless desirability scale d_i, defined as partial desirability function. The scaling is done so that d_i ranges between $d_i = 0$, for a completely undesired response, to $d_i = 1$ for fully desired response above which further improvements would have no importance. Therefore, the individual desirability functions are combined into an overall desirability function, D, that weights the responses together, with one single criterion. The values of D computed from the observed responses allow location of a near-optimum region.

For data calculation and treatment Nemrod W software [37] was used.

3 Experimental

3.1 Samples

Chromium was deposited on low carbon steel discs (∅ = 12 mm, S_{work} = 1.13 cm^2) from a commercial sulphate catalysed chromium bath purchased by Atotech (250 g L^{-1} CrO_3, 3 g L^{-1} H_2SO_4). Before plating, the steel substrate was mechanically polished with 1200 paper followed by 6 µm, 3 µm diamond finishing , and then depassivated in HCl 2mol L^{-1}.

A depositing thickness simulation using the Castor Elec 3D software, developed by the CETIM—France [38], permitted us to achieve deposit uniformity. The calculation of the current distribution by the boundary element method (BEM) [39, 40] allowed us to predict the profile change of the cathode during the electrodeposition process and to design the most appropriate electrolyser outfits and tools to obtain uniformity of the chromium thickness. Towards this end, an auxiliary electrode (low carbon steel ring with internal diameter 19 mm—external diameter 27 mm—thickness 2 mm) was introduced to the periphery of the cathode disc, to decrease the non-uniformity of the local current density (Fig. 2). The auxiliary electrode and the cathode were positioned in an insulating support, as in Fig. 3. Preliminary tests established a good correlation between the measured and calculated deposit thicknesses. Before optimisation, the non-uniformity of the layer could reach 30–45%, as the thickness at the edge was 41.1–42.5 µm, while in the centre the thickness was near 27.7 µm, and after optimisation, the values varied in the range 23.0–23.5 µm.

3.2 Measurement procedures

3.2.1 Roughness

A large number of useful factors are available to characterize the microgeometric properties of electrodeposit [41, 42]. The surface roughness average, R_a, and the mean value of the roughness, R, were taken as parameters defined as the arithmetical mean of the departures of the roughness profile from the mean line along the measurement and the average height of the motifs respectively. These definitions are set out in Eqs. (1) and (2):

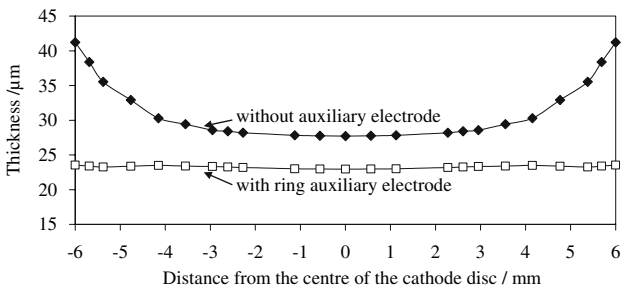

Fig. 2 Chromium thickness profile on the cathode with and without auxiliary electrode (ring- diameter 17 mm)

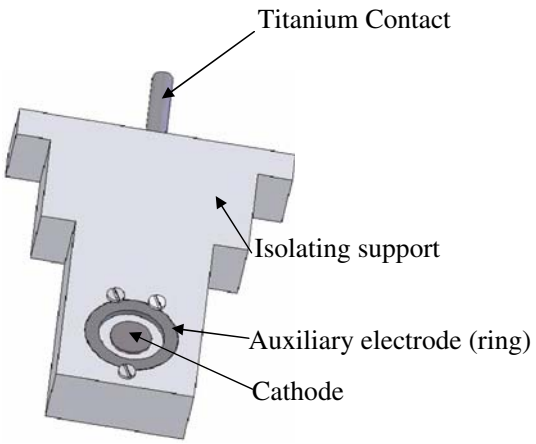

Fig. 3 Experimental cathodic support

$$R_a = \frac{1}{L}\int_{x=0}^{x=L} |z(x)|\, dx \tag{1}$$

and

$$R = \frac{1}{n}\sum_{i=1}^{i=n} R_i \tag{2}$$

where z(x) is the profile value of the roughness profile, L the evaluation length, R_i the height of the roughness design and n the number of R_i values .

The roughness was measured using an interferometer (WIKO optical device NT 2000).

3.2.2 Microhardness

The microhardness measurements were made using a SHIMADZU HMV-M3 testing machine at a load of 50 g.

3.2.3 Scratch test

The sclerometer principle is illustrated in Fig. 4. It consists of scoring a studied surface with a diamond indenter with specific geometry (conical in our case). This apparatus allows us to simulate the mechanisms of abrasion on the surface of materials. This process gives information on the dynamic behaviour of surfaces during a scratch by measurement of normal and tangential forces.

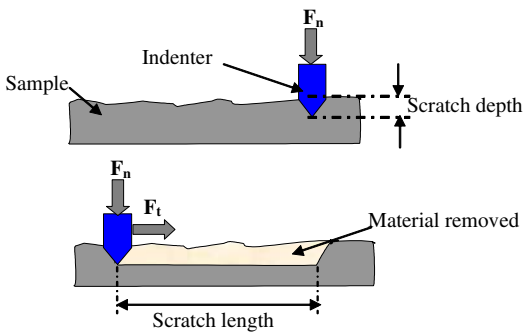

Fig. 4 Principle of the sclerometer

The test conditions imposed on the indenter are: a normal force of 5N, a displacement of 1 mm and a scratch velocity of 250 μm s^{-1}. The 3D scratch morphology was obtained using an optic profilometer (WIKO NT2000). The volume V_r was calculated using image analysis software. The specific abrasive energy E_s (μJ μm^{-3}) is the energy needed to remove a volume of material:

$$E_s = \frac{\int_0^l F_t(x)\cdot dx}{V_r} \tag{3}$$

where F_t is the tangential force, V_r the material volume removed and l, the length of the scratch.

3.3 Surface morphology techniques

Chromium topography images were obtained with a Nanoscope AFM (Digital Instrument Model di-3100) in air with a tapping mode using silicon tips (Model TESP) of 10–15 μm lengths. This model has a rectangular shaped cantilever 125 μm long with ca. 50 N m^{-1} force constant and ca. 325 kHz resonant frequency. The cone half angles were 10 degrees at the side, 25 degrees at the front and 10 degrees at the back. Typically a 1–3 lines s^{-1} scan speed was used for scanning on a 50 × 50 μm^2 area and 512 sampling numbers were used for each line.

4 Results and discussion

4.1 Response models and validation

Table 2 shows the second order design in coded variables and the obtained responses Y_i. The 31 observed responses are used to compute the model coefficients using the least square method [30–35]. The equations of the fitted models are:

$$\begin{aligned}\hat{Y}_1 = {} & 678.8 - 17.1X_1 + 13.0X_2 - 38.1X_3 + 19.0X_4 \\ & + 4.2X_5 + 5.9X_1X_2 - 22.6X_1X_3 - 19.1X_2X_3 \\ & + 20.9X_1X_4 - 46.6X_2X_4 - 7.3X_3X_4 - 22.4X_1X_5 \\ & - 15.4X_2X_5 - 17.2X_3X_5 - 54.2X_4X_5 + 7.3X_1^2 \\ & - 39.3X_2^2 - 13.7X_3^2 - 3.3X_4^2 - 36.3X_5^2\end{aligned} \tag{4}$$

Table 2 Experimental design in coded variables and measured responses

N_i	X_1	X_2	X_3	X_4	X_5	Y_1 Hv	Y_2 R_a	Y_3 R	Y_4 E_s
1	–1	–1	–1	–1	1	690	618	4.18	0.025
2	1	–1	–1	–1	–1	416	298	3.43	0.008
3	–1	1	–1	–1	–1	593	435	3.74	0.020
4	1	1	–1	–1	1	701	270	4.08	0.014
5	–1	–1	1	–1	–1	495	278	3.12	0.011
6	1	–1	1	–1	1	482	341	3.43	0.007
7	–1	1	1	–1	1	701	196	2.73	0.044
8	1	1	1	–1	–1	491	310	3.58	0.019
9	–1	–1	–1	1	–1	645	230	2.48	0.032
10	1	–1	–1	1	1	658	222	2.85	0.012
11	–1	1	–1	1	1	593	339	3.15	0.026
12	1	1	–1	1	–1	705	293	3.76	0.038
13	–1	–1	1	1	1	645	227	2.78	0.029
14	1	–1	1	1	–1	650	529	4.72	0.048
15	–1	1	1	1	–1	571	346	3.82	0.010
16	1	1	1	1	1	387	353	4.61	0.013
17	–2	0	0	0	0	709	357	3.29	0.019
18	2	0	0	0	0	725	380	4.21	0.026
19	0	–2	0	0	0	468	331	3.60	0.010
20	0	2	0	0	0	593	341	4.50	0.012
21	0	0	–2	0	0	717	263	3.21	0.020
22	0	0	2	0	0	549	304	3.15	0.020
23	0	0	0	–2	0	632	345	3.46	0.015
24	0	0	0	2	0	717	332	2.79	0.025
25	0	0	0	0	–2	590	358	4.83	0.028
26	0	0	0	0	2	495	373	3.93	0.014
27	0	0	0	0	0	675	353	3.49	0.015
28	0	0	0	0	0	701	359	3.46	0.013
29	0	0	0	0	0	675	348	3.20	0.014
30	0	0	0	0	0	689	332	3.57	0.015
31	0	0	0	0	0	636	368	3.60	0.010

$$\begin{aligned}\hat{Y}_2 = {} & 353.0 - 0.3X_1 - 7.5X_2 - 1.8X_3 - 9.7X_4 - 5.1X_5 \\ & - 7.9X_1X_2 + 64.1X_1X_3 - 8.7X_2X_3 + 35.2X_1X_4 \\ & + 27.9X_2X_4 + 54.2X_3X_4 - 20.9X_1X_5 - 18.7X_2X_5 \\ & - 33.7X_3X_5 - 22.6X_4X_5 + 3.2X_1^2 - 4.9X_2^2 \\ & - 18.0X_3^2 - 4.3X_4^2 + 2.5X_5^2 \end{aligned} \quad (5)$$

$$\begin{aligned}\hat{Y}_3 = {} & 3.51 + 0.26X_1 + 0.18X_2 + 0.04X_3 - 0.06X_4 \\ & - 0.11X_5 + 0.05X_1X_2 + 0.21X_1X_3 - 0.07X_2X_3 \\ & + 0.19X_1X_4 + 0.16X_2X_4 + 0.39X_3X_4 - 0.01X_1X_5 \\ & + 0.01X_2X_5 - 0.16X_3X_5 - 0.12X_4X_5 + 0.03X_1^2 \\ & + 0.10X_2^2 - 0.11X_3^2 - 0.13X_4^2 + 0.19X_5^2 \end{aligned} \quad (6)$$

$$\begin{aligned}\hat{Y}_4 = {} & 0.0130 - 0.0010X_1 + 0.0007X_2 + 0.0003X_3 \\ & + 0.0033X_4 - 0.0018X_5 + 0.0004X_1X_2 + 0.0015X_1X_3 \\ & - 0.0019X_2X_3 + 0.0041X_1X_4 - 0.0050X_2X_4 \\ & - 0.0014X_3X_4 - 0.0074X_1X_5 + 0.0023X_2X_5 \\ & + 0.0016X_3X_5 - 0.0050X_4X_5 + 0.0026X_1^2 \\ & - 0.0002X_2^2 + 0.0020X_3^2 + 0.0020X_4^2 + 0.0023X_5^2 \end{aligned} \quad (7)$$

Table 3 summarizes the analysis of variance (ANOVA) for the four responses. As can be seen, the regression sum of squares is statistically significant and none of them have a significant lack of fit [32–35]. These results are confirmed by the high values of the multiple correlation coefficient

Table 3 Analysis of variance (ANOVA) for the responses $\hat{Y}_1$, $\hat{Y}_2$, $\hat{Y}_3$ and $\hat{Y}_4$

Sources of variation	Sum of square	Degrees of freedom	Mean square	F. Ratio	Test F*
Hardness/Hv					
Regression	2.56619×10^5	20	1.28309×10^4	5.6816	H.S.
Residual	2.25832×10^4	10	2.25832×10^3	5.6253	
Lack of fit	2.01904×10^4	6	3.36507×10^3	5.6253	N.S
Pure error	2.39280×10^3	4	5.98200×10^2		
Total variation	2.79202×10^5	30			
Roughness average/R_a					
Regression	2.01475×10^5	20	1.00737×10^4	17.8271	H.S
Residual	5.65079×10^3	10	5.65079×10^2	4.5511	
Lack of fit	4.92879×10^3	6	8.21465×10^2	4.5511	N.S
Pure error	7.22000×10^2	4	1.80500×10^2		
Total variation	2.07126×10^5	30			
*Roughness/*R					
Regression	10.0773	20	0.5039	7.2546	H.S
Residual	0.6945	10	0.0695	3.9581	
Lack of fit	0.5944	6	0.0991	3.9581	N.S
Pure error	0.1001	4	0.0250		
Total variation	10.7718	30			
Specific energy of abrasion/E_s					
Regression	3.03037×10^{-3}	20	1.51518×10^{-4}	9.0422	H.S
Residual	1.67568×10^{-4}	10	1.67568×10^{-5}	5.8282	
Lack of fit	1.50368×10^{-4}	6	2.50613×10^{-5}	5.8282	N.S
Pure error	1.72000×10^{-5}	4	4.30000×10^{-6}		
Total variation	3.19794×10^{-3}	30			

* H.S: significant at the level 99%; $F_{0,01}(20,10) = 4,41$

N.S: non significant at the level 95%; $F_{0,05}(6,4) = 15,21$

squares (R^2): 0.92, 0.97, 0.94, 0.95 for $\hat{Y}_1$, $\hat{Y}_2$, $\hat{Y}_3$ and $\hat{Y}_4$ respectively. It should be noted that the R^2 values represent the percentage variation in the responses explained by the deliberate variation of the factors in the course of the experiments. From the overall results it can be concluded that each second order model is adequate and can be used as a prediction equation in the studied domain.

The optimum paths of the response surfaces for the fitted models are shown in Figs. 5–8. Examination of the obtained graphs allows us to deduce a set of coordinates corresponding to maxima for $\hat{Y}_1$ and $\hat{Y}_4$, and minima for $\hat{Y}_2$ and $\hat{Y}_3$ at the boundary of the studied domain (at a distance of 2 from the centre). These results are reported in Table 4.

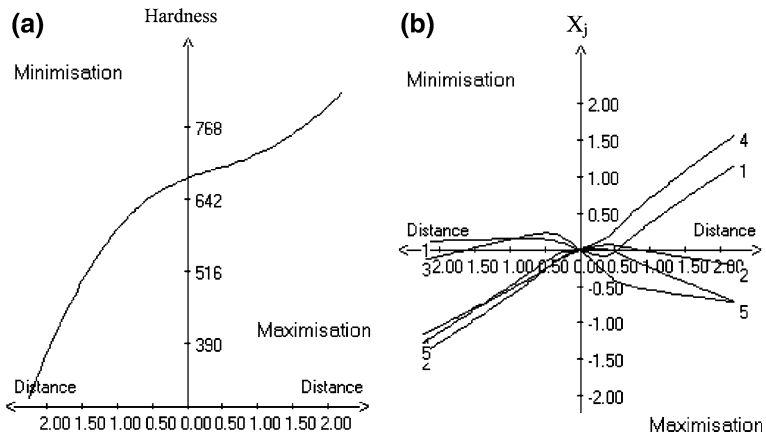

Fig. 5 (**a**) Optimum path of the response surface $\hat{Y}_1$ where ordinates represent the optimum response reached on the built spheres for radius R indicated in abscissas; (**b**) co-ordinates of the points of plot (a) for each factor in coded variables. The right part of both plots refers to the maximisation of the response; the left part of the plots refers to the minimisation of the response

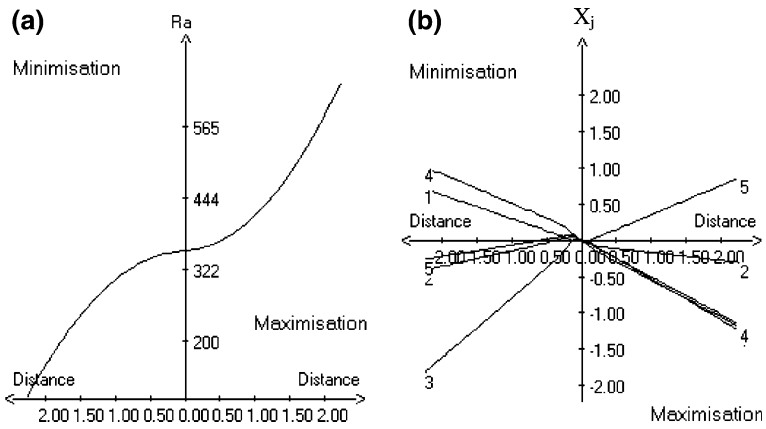

Fig. 6 (**a**) Optimum path of the response surface $\hat{Y}_2$ where ordinates represent the optimum response reached on the built spheres for radius R indicated in abscissas; (**b**) co-ordinates of the points of plot (a) for each factor in coded variables. The right part of both plots refers to the maximisation of the response; the left part of the plots refers to the minimisation of the response

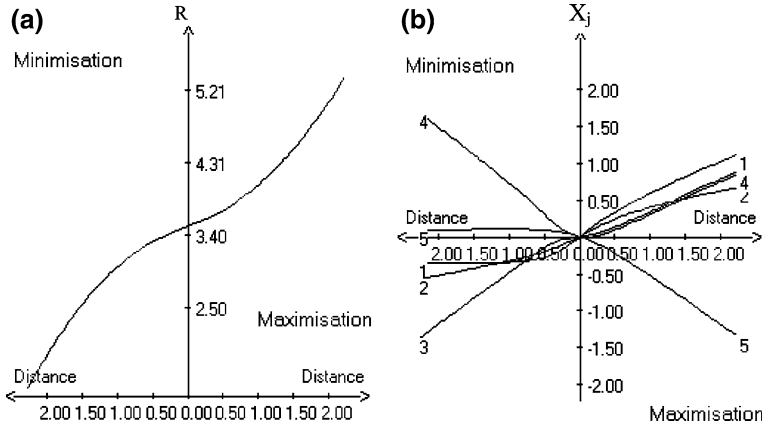

Fig. 7 (**a**) Optimum path of the response surface $\hat{Y}_3$ where ordinates represent the optimum response reached on the built spheres for radius R indicated in abscissas; (**b**) co-ordinates of the points of plot (a) for each factor in coded variables. The right part of both plots refers to the maximisation of the response; the left part of the plots refers to the minimisation of the response

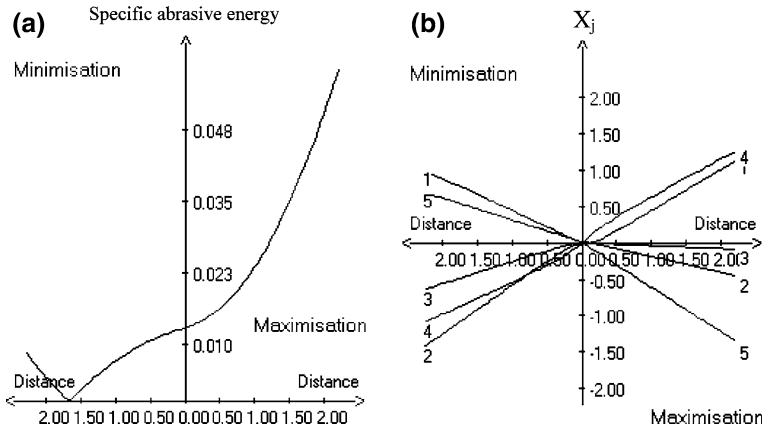

Fig. 8 (**a**) Optimum path of the response surface$\hat{Y}_4$ where ordinates represent the optimum response reached on the built spheres for radius *R* indicated in abscissas; (**b**) co-ordinates of the points of plot (a) for each factor in coded variables. The right part of both plots refers to the maximisation of the response; the left part of the plots refers to the minimisation of the response

By inspection of Table 4 it can be concluded that the individual analysis of the responses does not lead to clear common experimental conditions. Therefore a multicriteria methodology that looks for certain compromise experimental conditions fulfilling the expectations of the analyst is required.

4.2 Optimization

The search for experimental conditions, which optimize simultaneously the four responses, leads us to use desirability functions as proposed by Deringer and Swich [36].

For the four estimated responses, one-sized transformations are used and are shown in Figure 9, which also shows the undesirable responses and the fully desired responses.

Taking into account all the requirements for the four responses, we opted to compute an overall desirability measure D as a weighted geometric mean of the desirability values for individual parameters. At this stage, it is to be noticed that for tribological applications, the

Table 4 Set of co-ordinates corresponding to maxima for $\hat{Y}_1$ and $\hat{Y}_4$ and minima for $\hat{Y}_2$ and $\hat{Y}_3$ at the boundary of the studied domain (at a distance 2 from the centre)

	X_1	X_2	X_3	X_4	X_5	U_1 °C	U_2 A dm^{-2}	U_3 s	U_4 A dm^{-2}	U_5 ms
$\hat{Y}_1$	1	–0.1	0.7	1.5	–0.6	57.5	41.4	11.8	51.0	24.0
$\hat{Y}_2$	0.5	–0.3	–1.5	0.8	–0.2	53.8	40.2	3.0	46.8	28.0
$\hat{Y}_3$	–0.3	–0.5	–1.3	1.5	0.1	47.8	39.0	3.8	51.0	31.0
$\hat{Y}_4$	1	–0.3	0	1	–1.2	57.5	40.2	9.0	48.0	18.0

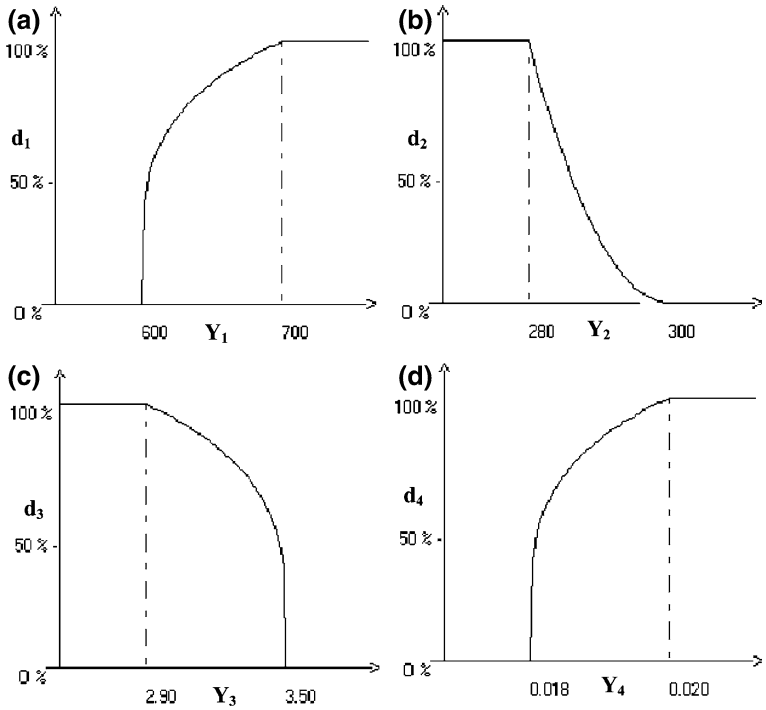

Fig. 9 Transformation response $\hat{Y}_i$ into desirability values d_i: (**a**) the hardness (Hv), (**b**) the roughness criteria R_a (nm), (**c**) the roughness criteria R(μm) and (**d**) the specific abrasive energy, E_s ($\mu J \cdot \mu m^{-3}$)

surface roughness average and the specific abrasive energy are considered among the most pertinent parameters. Therefore we choose to attribute different weights for the four studied responses: three for $\hat{Y}_2$, two for $\hat{Y}_4$, and one for $\hat{Y}_1$ and $\hat{Y}_3$. Consequently, the function D, over the experimental domain, is calculated using the equation:

$$D = (d_1\, d_2^3\, d_3\, d_4^2)^{1/7}. \quad (8)$$

The value of D is highest at conditions where a combination of the different criteria is globally optimal. After calculation by NEMROD software, the optimal experimental conditions are obtained (Table 5). Under these conditions, the estimated response values are 738 Hv,

Table 5 Optimal conditions

	X_j	U_j
Temperature of the plating bath (°C)	–0.015	49.9
Cathodic pulse current density J_c (A dm^{-2})	–0.006	42.0
On time or cathodic pulse length T_c (s)	–0.692	6.23
Anodic pulse current density J_a (A dm^{-2})	1.585	51.5
Reverse on time or anodic pulse length T_a (ms)	–0.149	28.5

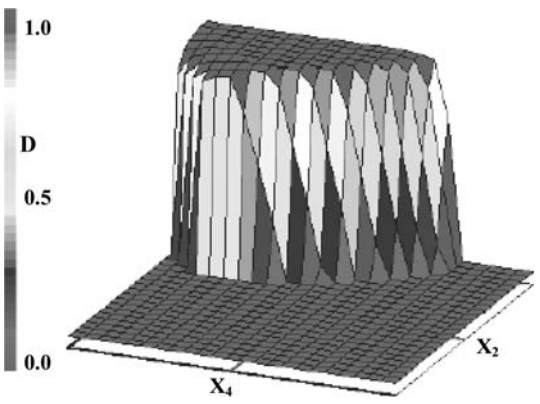

Fig. 10 Graphical representation of the overall desirability function D. X_2 is plotted against X_4 maintaining U_1 at 50 °C, U_3 at 6.2 s and U_5 at 28.5 ms

Table 6 Range of variables around the optimum

	Low limit		Upper limit	
	$X_j(-)$	$U_j(-)$	$X_j(+)$	$U_j(+)$
Temperature of the plating bath (°C)	–0.240	48.2	0.350	52.63
Cathodic pulse current density J_c (A dm^{-2})	–0.008	41.95	0.283	43.70
On time or cathodic pulse length T_c (s)	–0.900	5.4	–0.500	7.0
Anodic pulse current density J_a (A dm^{-2})	1.450	44.70	1.800	52.8
Reverse on time or anodic pulse length T_a (ms)	–0.165	28.35	0.200	32.00

262 nm, 2.61 μm and 0.027 μJ μm^{-3} for hardness, R_a, R and specific abrasive energy respectively, validated experimentally.

The resulting contour plot from modelling the overall desirability function can be seen in Figure 10 which shows a rather flat area around the optimal conditions, which means that the optimum is not just one point but a volume around this point. This volume can be roughly defined by giving a range of variation of each variable in accordance with the results of the desirability study (Table 6). This illustrates the robustness of the predicted optimal conditions.

4.3 Surface morphology

In order to assess surface morphology, the chromium coatings were analysed by AFM. It is important to point out that, as a part of this study, a relatively smooth surface (i.e. fine-grained deposit) is needed to ensure a low coefficient of friction without further mechanical treatment.

Figure 11a–c display three typical morphologies. The deposits exhibit a distinctively rough surface structure. Separate crystallites are clearly visible. The surface morphology appears to be a set of continuous mounds, which are strongly affected by the experimental conditions. The grains are pyramidal, square or nodular in shape in accordance with the variations of the pulse factors. On the whole, it seems that a decrease in the reverse time (or in the reverse current) promotes the growth of large separate

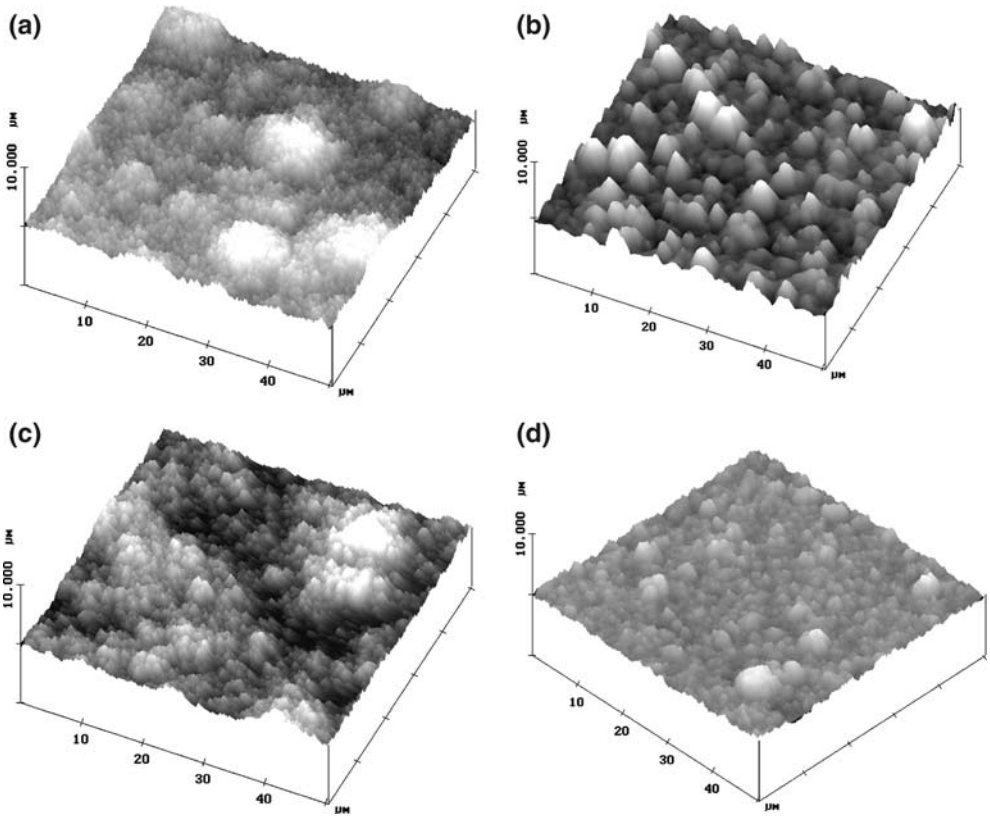

Fig. 11 The tapping mode atomic force microscopy (TM-AFM) images of chromium electrodeposits obtained at various operating pulse plating conditions. Scan size is 50 × 50 μm. (**a**) experiment N_1—U_1 42.5 °C, U_2 at 36 A dm^{-2}, U_3 at 5 s, U_4 at 36 A dm^{-2} and U_5 at 40 ms, (**b**) experiment N_{16}—U_1 57.5 °C, U_2 at 48 A dm^{-2}, U_3 at 13 s, U_4 at 48 A dm^{-2} and U_5 at 40 ms, (**c**): experiment N_{25}—U_1 50 °C, U_2 at 42 A dm^{-2}, U_3 at 9 s, U_4 at 42 A dm^{-2} and U_5 at 10 ms, (**d**) experiment under optimum conditions—U_1 50 °C, U_2 at 42 A dm^{-2}, U_3 at 6.2 s, U_4 at 51.5 A dm^{-2} and U_5 at 28.5 ms

crystallites (Fig. 11c). In addition, the morphology of the electrodeposit obtained under the optimal conditions (Table 5) has been analysed (Fig. 11d). The coating exhibits a nodular fine-grained morphology which agrees with the values of the roughness parameters.

It is noteworthy that, for all the pulse plating experiments, there is no evidence of any microcracking unlike in DC plating coatings [13–15]. This can be explained by the re-oxidation of hydrogen dissolved in the deposit, during the reversal step, thus reducing the tendency for cracking.

5 Conclusion

In this study a central composite design experiment was used to check the effect of the electroplating parameters (electrolyte temperature, cathodic and anodic pulse current densities, and cathodic and anodic pulse lengths) on four properties of hard chromium electrodeposits, namely the hardness (Hv), the roughness quantified by the two criteria R_a (nm) and R (μm)), and the specific abrasive energy, E_s (μJ μm^{-3}). Individual analysis of the responses revealed that there were no common experimental conditions which fulfilled the required properties. Therefore a compromise was reached using the desirability function.

Its coordinates are: temperature of the plating bath: 49.9 °C; cathodic pulse current density: 42.0 A dm^{-2}; anodic pulse current density: 51.5 A dm^{-2}, cathodic pulse length: 6.23 s and anodic pulse length: 28.5 ms. Under these conditions the estimated response values are 738 Hv, 262 nm, 2.61 μm and 0.027 μJ μm^{-3} for hardness, R_a, R and specific abrasive energy respectively. The corresponding coating, examined by AFM, exhibits a nodular fine-grained morphology.

Acknowledgements The authors thank Mr James Evershed for his assistance and Mrs C. Millot - Roques Carmes and Dr. J. Gayolle for conducting SEM and AFM analyses, respectively.

References

1. Dennis IK, Such TE (1993) In: Nickel and chromium plating, 3rd edn. Woodhead Publishing, Cambridge
2. Weiner R, Walmsley A (1980) In: Chromium plating. Finishing Publications
3. Strattford KN, Datta PK, Googan CG (1990) In: Coatings and surface treatment for corrosion and wear resistance. Ellis Horwood
4. Tyler JM (1995) Metal Finish 10:11
5. Hoare JP (1983) J Electrochem Soc 130:1475
6. Mandich NV (1997) Plat Surf Finish 84:97
7. Socha J (1999) Galvanotechnik 90:2976
8. Rashlov ST, Stoichev DS, Tomov I (1972) Electrochim. Acta 17:1955
9. Finch GI, Quarrel AG, Wiman H (1935) Trans. Faraday Soc 31:1051
10. Finch GI (1950) Electrochem 54:457
11. Snavely CA (1947) Trans Electrochem. Soc 92:537
12. Pangorov NA (1965) J. Electroanal. Chem 9:70
13. Morisset P. (1993) Chromage dur et décoratif, CETIM
14. Martyak NM, Mc Caskie JE, Voos B, Pileth W (1997) J. Materials Science 36:6069
15. Durut F, Benaben P, Forest B, Rieu J (1998) Metal Finishing 3:52
16. Bergenstof Nielsen C, Leisner P, Lorsewell A (1998) J. Applied Electrochemistry 28:141
17. Tsai RY, Wu ST (1990) J Electrochem Soc 137:3057
18. Gaigner G, Assoul M, Wery M, Pagetti J (2001) IIIrd International Colloquium, Bulletin du Cercle d'Etudes des Métaux, Tome XVII, Sept St Etienne (France)
19. Leisner P, Bech-Nielsen G, Moller P (1993) J. Applied Electrochemistry 23:1232
20. Leisner P, Ulrich D, Moller P (1992) Plat. Surf. Finish 79:62
21. Clauberg W (1989) Metalloberflache 43:9
22. Roy S, Landolt D (1997) J. Applied Electrochemistry 27:299
23. Chene O, Landolt D (1989) J. Applied Electrochemistry 19:188
24. Ibl N, Puippe JC (1978) Angerer H. Surf. Technol 6:287
25. Ibl N (1980) Surf Technol 10:81
26. Chen HY (1971) J Electrochem Soc 118:551
27. Chin DT (1983) J Electrochem Soc 130:1657
28. Choi Y, Kim M, Kwon SC (2003) Sur Coatings Technol 169–170:81
29. Choi Y, Baik NI, Hong SI (2001) Thin Solid Films 397:24
30. Box EP, Hunter WG, Hunter JS (1978) In: Wiley J (ed) Statistics for experimenters. New York
31. Myers RH, Montgomery DC (1995) In: Wiley J (ed) Response surface methodology: process and product optimization using designed experiments. New York
32. Goupy J (1999) In: Dunod (ed) Plans d'Expériences pour Surfaces de Réponse. Paris, 1999
33. Khuri AI, Cornell JA (1996) In: Dekker M (ed) Response surfaces: design and analyses. 2nd edn. New York
34. Mathieu D, Phan Tan-Luu R (1997) In: Technip (ed) Plans d'Expériences: Application à l'entreprise. Paris
35. Lewis GA, Mathieu D, Phan-Tan-Luu R (1999) In: Dekker M (ed) Pharmaceutical experimental design. New York
36. Derringer G, Suich R (1980) J Qual Tech 12:214
37. Mathieu D, Nony J, Phan Tan-Luu R (2002) NEMROD-W software. LPRAI, Marseille
38. CASTOR Elec 3D software, CETIM, Senlis
39. Brebbia CA, Domingues J (1989) In: Boundary elements – an introducing course, Mc Graw Hill Book Co, New York
40. Druesne F, Paumelle P, Villon P (1999) Eur Rev Finite Elements 1:8
40. DIN 4768/1 ''Determination of Surface Roughness of Parameters Ra, Rz, and Rmax by means of electrical stylus instruments'', published by the Deutsche Institut fuer Normung e.V. , 1987
42. ISO 4287/1997, Geometrical Product Specifications (GPS) – Surface Texture: Profile Method –Terms, Definition and Surface Texture Parameters, International Organisation of Standardisation, Geneva, 1997